

Fracture Mechanics Analysis in 2-D Anisotropic Thermoelasticity Using BEM

Y.C. Shiah¹, C.L. Tan¹

Abstract: In the direct formulation of the boundary element method (BEM), a volume integral arises in the resulting integral equation if thermal effects are present. The steps to transform this volume integral into boundary ones in an exact analytical manner are reviewed in this paper for two-dimensional anisotropic thermoelasticity. The general applicability of the BEM algorithm for fracture mechanics applications is demonstrated by three crack problems with slanted cracks. The numerical results of the stress intensity factors are presented and compared with those obtained using superposition.

keyword: BEM, anisotropy, thermoelasticity, fracture mechanics

1 Introduction

Since the early 1960's, structural materials with anisotropic properties have been widely used in numerous commercial, aerospace, and military engineering applications. Many of these applications involve changes in the temperature of the engineering component. This has led to increasing attention being paid to the thermoelastic analysis of such materials when they are subject to thermal loads. Although some analytical solutions have been obtained for a few specific problems, recourse to numerical methods such as the finite element method (FEM) and the boundary element method (BEM) is usually necessary in general. To this end, the BEM, sometimes also referred to as the boundary integral equation (BIE) method, has been recognized as an efficient computational tool for engineering stress analysis, especially for problems with rapidly varying stresses, such as those occurring near cracks. It has the distinctive feature that only the boundary of the numerical solution domain needs to be modeled, in contrast to domain-type numerical schemes such as the FEM.

In the basic form of the direct formulation of the BEM for elastostatics with body force or thermal effects, extra volume integral terms arise in the integral equation. For isotropic elasticity, several schemes have been proposed to deal with these extra volume integral terms over the years. They include the Monte Carlo and domain fanning approach [see, e.g., Gipson and Camp (1985); Camp and Gipson (1992)], the particular integral approach [see, e.g., Lachat (1975); Deb and Barnerjee (1990)], and the exact transformation method (ETM) [see, e.g., Rizzo and Shippy (1977); Tan (1983); Danson (1983)].

Among these approaches, the exact transformation method is most appealing as it transforms the volume integrals into surface ones without incurring any analytical approximations. Thus the notion of the BEM being a boundary solution technique becomes fully restored. The key to the success of this transformation is the canonical form of the governing heat conduction equation in isotropy which is the simple Poisson's equation.

Due to the fact that the fundamental solutions for anisotropic elastic solids are mathematically much more complicated than those for isotropic ones, similar exact transformations for anisotropic elasticity have not been successfully achieved until very recently. The works of Zhang, Tan and Afagh (1996a, 1996b, 1997) represent perhaps the first reported successful attempts using the ETM to deal with body forces in anisotropic elasticity. This work was subsequently extended by the present authors to obtain interior point solutions using the BEM when body forces are present, Shiah and Tan (1998a). Although thermal effects can, in essence, be treated as an effective body force over the solution domain in Navier's equations of equilibrium [see, e.g., Sokolnikoff (1956)], the process of the volume-to-surface integral transformation is not as straightforward. This is due to mathematical difficulties stemming from the governing heat conduction equation in anisotropy, namely,

$$k_{ij}T_{,ij} = C_o \quad (1)$$

In Eq. 1, C_o is the heat source term and k_{ij} are the heat conductivity coefficients of the material. The exact transformation of the volume integral associated with thermal effects for anisotropic solids in BEM, was successfully carried out by the present authors only very recently, Shiah and Tan (1999a). A direct domain mapping technique [see Shiah and Tan (1998b)], was employed to first transform Eq. 1 into

$$T_{,\underline{ii}} = C_1 \quad (2)$$

where $C_1 = C_o k_{11} / \Delta$ and $\Delta = k_{11} k_{22} - k_{12}^2$. The underline in the indices appearing in Eq. 2 denotes a new coordinate system defined in Eq. 7 and Eq. 8 below. It is perhaps worth noting that the particular integral approach has also been employed by Deb, Henry, and Wilson (1991) to deal with the volume integral term in anisotropic elasticity. However, for general temperature distributions, this scheme involves sub-dividing the domain and carrying out multiple regression analyses to approximate the temperature field in each of the sub-domains as simple polynomials. The accuracy of the solution will evi-

¹ Department of Mechanical & Aerospace Engineering, Carleton University, Ottawa, Canada K1S 5B6

dently depend upon the particular integrals chosen, and special ones will need to be derived for problems with cracks.

Several researchers have used the BEM for the fracture mechanics analysis of an anisotropic body under mechanical loads over the past several years [see, e.g., Snyder and Cruse (1975); Kamel and Liaw (1981); Tan and Gao (1992); Tan, Gao, and Afagh (1992); Sollero and Aliabadi (1993); Pan and Amadei (1996)]. However, similar BEM works for crack problems involving thermal loads are extremely scarce. Recently, the authors have presented a verification of the validity of the ETM approach for three simple symmetric crack configurations under thermal loading, Tan and Shiah (1999). The BEM algorithm was checked by comparing the solutions obtained using quasi-isotropic material properties with those obtained from the BEM algorithm for pure isotropy.

The aim of this paper is to provide a more elaborate demonstration of the applicability of this ETM approach in its ability to treat the general thermoelastic fracture problem in 2D anisotropic elasticity. Plates with inclined cracks are considered in this study and the results of the stress intensity factors are compared with those obtained using a method of superposition. In the next section, the basic equations of the BEM in 2D anisotropic elasticity are presented. This is followed by a review of the key steps in the ETM to transform the volume integral associated with thermal effects into boundary ones. The general capability of this BEM approach for fracture mechanics analysis is then illustrated by three examples.

2 2-D anisotropic thermoelastic BIE

In the direct formulation of the BEM for an anisotropic solid in two-dimensions, the displacements, u_i , and the tractions, t_i , on the boundary S of the domain Ω , can be shown to be related to each other by the following integral equation,

$$C_{ij}u_i(P) + \int_S u_i(Q)T_{ij}(P, Q) dS = \int_S t_i(Q)U_{ij}(P, Q) dS + \int_{\Omega} X_i(q)U_{ij}(P, q) d\Omega \quad (3)$$

where Q and q represent the field points on S and in Ω , respectively, and P represents the source point on S . In Eq. 3, X_i represents the equivalent body-force term contributed by the temperature change in the domain, and $U_{ij}(P, q)$ is the displacement fundamental solution, given by

$$U_{ij}(P, q) = 2\Re \{ r_{i1}A_{j1} \log z_1 + r_{i2}A_{j2} \log z_2 \} \quad (4)$$

Also, $T_{ij}(P, Q)$ is the corresponding traction fundamental solution [see, e.g., Tan, Gao and Afagh (1992)]. In Eq. 4, r_{ij} and A_{ji} are material constants and are complex quantities (Lekhnitskii (1981)); $\Re\{ \cdot \}$ is the operator which takes the real part of these quantities; and z_i is a generalised complex variable defined in terms of the characteristic roots, μ_i , and the difference of coordinates between the field point $Q(x_1, x_2)$ and the load

or source point $P(x_{p1}, x_{p2})$ as follows

$$z_i = (x_1 - x_{p1}) + \mu_i(x_2 - x_{p2}) = \zeta_1 + \mu_i\zeta_2 \quad (5)$$

In Eq. 5, ζ_i represent the local coordinates which have the origin located at the source point. If the temperature change of the elastic body is Θ , the equivalent body-force X_i can then be written as $X_i = -\gamma_{ij}\Theta_{,j}$ where γ_{ij} are the coefficients related to the thermal properties of the anisotropic body. Substituting this and the additional thermal traction term into Eq. 3, the complete integral equation considering thermal effects can be expressed as

$$C_{ij}u_i(P) + \int_S u_i(Q)T_{ij}(P, Q) dS = \int_S t_i(Q)U_{ij}(P, Q) dS + \int_S \gamma_{ik}n_k\Theta U_{ij}(P, Q) dS - \int_{\Omega} \gamma_{ik}\Theta_{,k}U_{ij}(P, q) d\Omega \quad (6)$$

where n_k is the unit outward normal at the field point on the boundary. It is obvious that the last term of the domain integral in Eq. 6 would destroy the distinctive feature of the BEM as a truly boundary solution computational technique if it is implemented directly. The task then is to analytically transform the domain integral into boundary ones. This will now be described.

3 Transformation of the domain integral

Only the main steps of the exact transformation process will be described here as its complete detail has been presented previously in the authors' recent paper, Shiah and Tan (1999a). The first step, before carrying out the actual integral transformation, is to map the physical domain into a new \hat{x}_i -coordinate system so that the governing heat conduction equation, Eq. 1, becomes the simple form of the Poisson's equation, Eq. 2, in the new coordinate system. This can be achieved by letting

$$\hat{x}_1 = \frac{\sqrt{\Delta}}{k_{11}}x_1 \quad (7)$$

$$\hat{x}_2 = x_2 - \frac{k_{12}}{k_{11}}x_1 \quad (8)$$

Figure 1 shows an example of the distortion of the physical domain in such a coordinate transformation. Here, a circular domain becomes mapped into an oblique ellipse in the transformed coordinate system.

The temperature gradients in the original Cartesian coordinate system may then be expressed in terms of the same in the mapped coordinate system (denoted by the underline in the indices) as follows,

$$\Theta_{,1} = \Theta_{,\underline{1}}\sqrt{\Delta}/k_{11} - \Theta_{,\underline{2}}k_{12}/k_{11} \quad (9)$$

$$\Theta_{,2} = \Theta_{,\underline{2}} \quad (10)$$

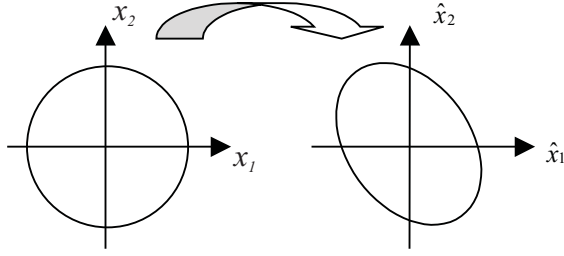


Figure 1 : Domain mapping into the \hat{x}_i -coordinate system

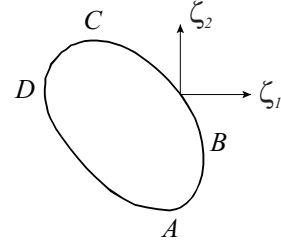


Figure 2 : A simply connected convex domain

From these, it can be readily shown that the extra volume integral (V.I.) in Eq. 3 can be rewritten as

$$(V.I.)_j = - \int_{\Omega} \gamma_{ik} \Theta_{,k} U_{ij} d\hat{\Omega} \quad (11)$$

where γ_{ik} can be expressed in a matrix form as

$$\gamma_{ik} = \begin{pmatrix} \gamma_{11} & (-\gamma_{11}k_{12} + \gamma_{12}k_{11})/\sqrt{\Delta} \\ \gamma_{21} & (-\gamma_{21}k_{12} + \gamma_{22}k_{11})/\sqrt{\Delta} \end{pmatrix} \quad (12)$$

By applying Green's theorem consecutively together with the auxiliary condition of Eq. 2, it can be shown that the volume integral, Eq. 11, can be analytically transformed into boundary ones as follows,

$$(V.I.)_j = \int_{\hat{S}} \left[(\gamma_{ik} Q_{ijk,l} \Theta - \gamma_{ik} Q_{ijk} \Theta_{,l} + C_1 \gamma_{ik} R_{ijkt}) n_l - \gamma_{ik} U_{ij} \Theta n_k \right] d\hat{S} \quad (13)$$

where the functions Q_{ijk} , $Q_{ijk,l}$, and R_{ijkt} in the integrand can be expressed in the forms below:

$$Q_{ijk} = 2\Re \left\{ r_{i1} A_{j1} \mu_{k1} z_1 \log(z_1) / (\mu_{11}^2 + \mu_{21}^2) + r_{i2} A_{j2} \mu_{k2} z_2 \log(z_2) / (\mu_{21}^2 + \mu_{22}^2) \right\} \quad (14)$$

$$Q_{ijk,l} = 2\Re \left\{ r_{i1} A_{j1} \mu_{k1} \mu_{l1} z_1 \log(z_1) / (\mu_{11}^2 + \mu_{21}^2) + r_{i2} A_{j2} \mu_{k2} \mu_{l2} z_2 \log(z_2) / (\mu_{21}^2 + \mu_{22}^2) \right\} \quad (15)$$

$$R_{ijkt} = 2\Re \left\{ \frac{r_{i1} A_{j1} \mu_{k1} (z_1^2 \log(z_1) - z_1^2/2)}{4\mu_{l1} (\mu_{11}^2 + \mu_{21}^2)} + \frac{r_{i2} A_{j2} \mu_{k2} (z_2^2 \log(z_2) - z_2^2/2)}{4\mu_{l2} (\mu_{21}^2 + \mu_{22}^2)} \right\} \quad (16)$$

In Eqs. 14-16, μ_{ji} takes the values of the elements of the following matrix:

$$\mu_{ji} = \begin{pmatrix} (k_{11} + \mu_1 k_{12})/\sqrt{\Delta} & (k_{11} + \mu_2 k_{12})/\sqrt{\Delta} \\ \mu_1 & \mu_2 \end{pmatrix} \quad (17)$$

With the domain integral transformed into boundary ones albeit in the mapped coordinate system, the BIE when thermal effects are considered, can now be expressed as follows:

$$\begin{aligned} C_{ij} u_i(P) + \int_S u_i(Q) T_{ij}(P, Q) dS \\ = \int_S t_i(Q) U_{ij}(P, Q) dS + \int_S \gamma_{ik} n_k \Theta U_{ij}(P, Q) dS \\ + \int_{\hat{S}} \left[(\gamma_{ik} Q_{ijk,l} \Theta - \gamma_{ik} Q_{ijk} \Theta_{,l} + C_1 \gamma_{ik} R_{ijkt}) n_l \right. \\ \left. - \gamma_{ik} U_{ij}(P, Q) \Theta n_k \right] d\hat{S} \end{aligned} \quad (18)$$

The integrands in the transformed integrals do not present numerical difficulties for their evaluation, as they are at most weakly singular. Before the numerical implementation, however, the validity of the analytical transformation needs to be further examined. Consider, for example, the instance when the source point is on that part of the boundary at which the negative ζ_1 -axis, the default branch cut of the multiple-valued function $\log(z)$, intersects the domain, as shown in Fig. 2.

The discontinuity along the branch cut invalidates the application of the Green's theorem above. If the domain is a simply-connected convex region as shown in the figure, this problem can be easily resolved by redefining the range of $\arg(z)$ as $0 < \arg(z) \leq 2\pi$ for all source points located along the side ABC . By this argument redefinition, the branch cut is actually reset to the positive ζ_1 -axis. However, this argument redefinition cannot be used to overcome the discontinuity problem of the $\log(z)$ term in the integrands for a simply connected non-convex domain such as the one shown in Fig. 3.

It is obvious that along the concave segment AB , the discontinuity problem cannot be resolved, irrespective of whether the negative or the positive ζ_1 -axis is chosen as the branch cut. As proposed by Zhang, Tan, and Afagh (1996a), if the outward normal n at an arbitrary source point is not directed towards any part of the domain, this difficulty can be easily overcome by redefining the principal value of $\arg(z)$ to be

$$(\beta - 2\pi) < \arg(z) \leq \beta \quad (19)$$

where β , defined in the range of $[0, 2\pi]$, denotes the inclined angle of the outward normal measured from the x_1 -axis. It

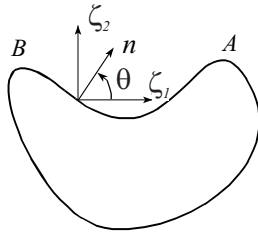


Figure 3 : A simply connected non-convex domain

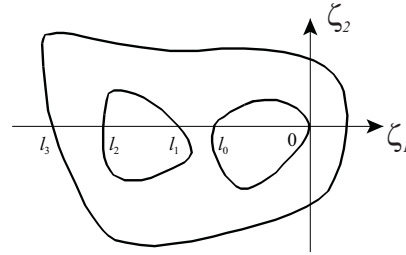


Figure 4 : A multiply connected domain

is also evident that this argument redefinition technique cannot always be applied to treat a simply-connected domain with an arbitrary shape or even a multiply-connected region intersected by the negative ζ_1 -axis at (l_0, l_1) and (l_2, l_3) as shown in Fig. 4.

To resolve this problem, an infinitesimal strip of the domain about the discontinuity along the branch cut is removed and the usual limiting process to restore this strip is followed, as described in Zhang, Tan, and Afagh (1996b) for body-force loading. For a general multiply-connected domain intersected by the negative ζ_1 -axis m times in the intervals $(l_{2m-1}, l_{2m-2}), (l_{2m-3}, l_{2m-4}), \dots (l_1, l_0)$, the complete BIE for plane anisotropic thermoelasticity can be shown to have the following form,

$$\begin{aligned}
 C_{ij}u_i(P) + \int_S u_i(Q)T_{ij}(P,Q) dS \\
 = \int_S t_i(Q)U_{ij}(P,Q) dS + \int_S \gamma_{ik}n_k \Theta U_{ij}(P,Q) dS \\
 + \int_{\hat{S}} \left[\left(\gamma_{ik}Q_{ijk,l} \Theta - \gamma_{ik}Q_{ijk} \Theta_{,l} + C_1 \gamma_{ik} R_{ijkl} \right) n_l \right. \\
 \left. - \gamma_{ik} U_{ij}(P,Q) \Theta n_k \right] d\hat{S} + \sum_{n=1}^m \int_{l_{2n-1}}^{l_{2n-2}} L_j(\zeta_1) d\zeta_1 \quad (20)
 \end{aligned}$$

where the integrand, $L_j(\zeta_1)$, for the extra line integrals is

$$\begin{aligned}
 L_j(\zeta_1) = 4\pi \Theta \gamma_{ik} \left(\frac{k_{12}}{k_{11}} \mathfrak{S} \left\{ \frac{r_{i1} A_{j1} \mu_{11} \mu_{k1}}{\mu_{11}^2 + \mu_{21}^2} + \frac{r_{i2} A_{j2} \mu_{12} \mu_{k2}}{\mu_{12}^2 + \mu_{22}^2} \right\} \right. \\
 \left. + \frac{\sqrt{\Delta}}{k_{11}} \mathfrak{S} \left\{ \frac{r_{i1} A_{j1} \mu_{21} \mu_{k1}}{\mu_{11}^2 + \mu_{21}^2} + \frac{r_{i2} A_{j2} \mu_{22} \mu_{k2}}{\mu_{12}^2 + \mu_{22}^2} \right\} \right) \\
 - 4\pi \gamma_{ik} \left(\frac{k_{12}}{k_{11}} \Theta_{,1} + \frac{\sqrt{\Delta}}{k_{11}} \Theta_{,2} \right) \zeta_1 \mathfrak{S} \left\{ \frac{r_{i1} A_{j1} \mu_{k1}}{\mu_{11}^2 + \mu_{21}^2} + \frac{r_{i2} A_{j2} \mu_{k2}}{\mu_{12}^2 + \mu_{22}^2} \right\} \\
 + C_1 \pi \zeta_1^2 \gamma_{ik} \left(\frac{k_{12}}{k_{11}} \mathfrak{S} \left\{ \frac{r_{i1} A_{j1} \mu_{k1}}{\mu_{11}(\mu_{11}^2 + \mu_{21}^2)} + \frac{r_{i2} A_{j2} \mu_{k2}}{\mu_{12}(\mu_{12}^2 + \mu_{22}^2)} \right\} \right. \\
 \left. + \frac{\sqrt{\Delta}}{k_{11}} \mathfrak{S} \left\{ \frac{r_{i1} A_{j1} \mu_{k1}}{\mu_{21}(\mu_{11}^2 + \mu_{21}^2)} + \frac{r_{i2} A_{j2} \mu_{k2}}{\mu_{22}(\mu_{12}^2 + \mu_{22}^2)} \right\} \right) \\
 - 4\pi \Theta \left(\frac{k_{12}}{k_{11}} \gamma_{i1} + \frac{\sqrt{\Delta}}{k_{11}} \gamma_{i2} \right) \mathfrak{S} \{ r_{i1} A_{j1} + r_{i2} A_{j2} \} \quad (21)
 \end{aligned}$$

In Eq. 21, $\mathfrak{S}\{ \cdot \}$ is the operator that takes the imaginary part of the complex quantities in the parentheses. With all discontinuities removed from the domain, equation (20) is thus analytically exact for any physical domain. It can be solved for the boundary unknowns in the usual manner in conventional BEM analysis. The numerical evaluation of the extra line integrals with the integrand of Eq. 21 presents no serious difficulty *per se*. However, it requires the temperature field data along the negative ζ_1 -axis for each source point along the boundary, if this axis cuts through the domain. This can be quite cumbersome in practice. A simple way to obviate this altogether is to use sub-regioning of the domain in the BEM analysis. It is also commonly used to treat crack problems in BEM analysis, as is the case in this study. By making the judicious choice of the sub-region interface boundaries, the argument redefinition given by Eq. 19 can be applied for each sub-domain.

The major advantages of the ETM approach over the particular integral approach are now evident. Not only is this scheme capable of dealing with general temperature distributions without incurring further numerical approximations, it can also be directly applied to crack problems. This capability of dealing with the thermoelastic crack problem will be illustrated next by three numerical examples.

4 Numerical Examples

Figure 5 show the three example problems considered in this study. They are thin, long rectangular plates, each containing an inclined crack. The width of each plate is W and its length is taken to be four times its width. In the first example, the plate has a central crack and in the second example, the plate has an edge crack. The third example is a plate with an inclined crack emanating from a central hole of radius $0.1W$. The length of the crack is a in all these examples.

With reference to Fig. 5, the two opposite ends, AB and CD, of the plate are assumed to be constrained in the x_2 -direction and free to move in the x_1 -direction in all these examples. The

Table 1 : Material properties of the glass/epoxy

E_{11}^*	E_{22}^*	ν_{12}^*	G_{12}^*	$\eta_{12,1}^*$	$\eta_{12,2}^*$
55	21	0.25	9.7	0	0
GPa	GPa		GPa		
α_{11}^*		α_{22}^*	K_{11}^*/K_{22}^*		
6.3E-6		2.0E-5	3.46/0.35		
/°C		/°C			

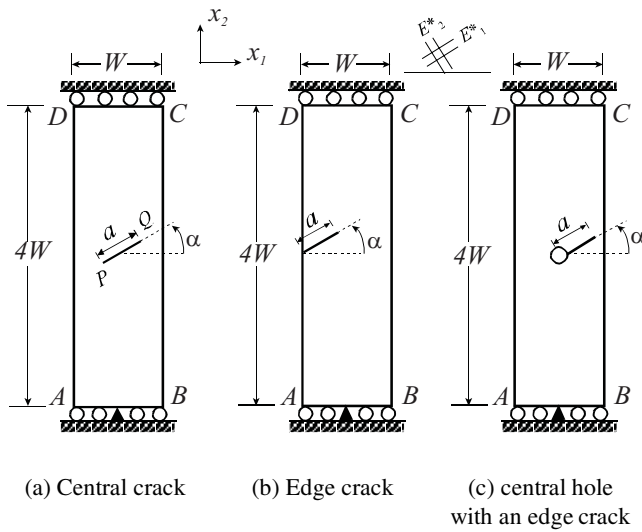


Figure 5 : Long rectangular plates: Examples (a) ~ (c)

plate has a steady-state temperature field which corresponds to the following thermal boundary conditions: the sides BC, AD and the crack surfaces, as well as the hole in Example (c), are assumed to be thermally insulated; the side AB is maintained at its original temperature but the side CD is cooled by temperature Θ_0 . The material properties in all cases are arbitrarily chosen to correspond to those of a glass/epoxy. Following the usual notations for the material properties but with the asterisks denoting values in the directions of the principal material axes, they are listed in Table 1.

As is usual for analysing any statically coupled thermoelastic problem, the associated anisotropic temperature field problem is first solved for the temperature and its gradient at all the boundary nodes. This is carried out using the direct domain mapping technique (see Shiah and Tan (1998a)) in conjunction with the conventional BEM for potential theory. The temperature field data so obtained are then used in the subsequent numerical stress analysis. As mentioned previously, the conventional sub-regioning technique in BEM is employed for treating the crack problems, whereby the sub-region boundaries lie on the plane of the crack. This also allows the branch

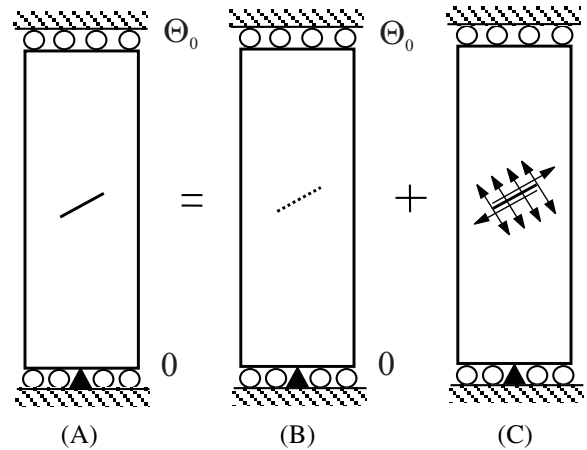


Figure 6 : Principle of superposition

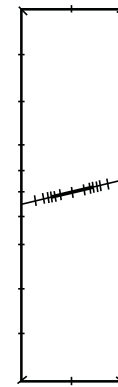


Figure 7 : Typical BEM mesh for Example (a)

cut of the $\log(z)$ term to be properly chosen so that it does not cut through the sub-domain, using the argument redefinition scheme with Eq. 19. This scheme has been implemented in the BEM code that was used in the present study which is based on the quadratic isoparametric formulation. Also, quarter-point crack-tip elements employed for the fracture mechanics analysis and the stress intensity factors are calculated using the well established “traction formula” in BEM (Tan and Gao (1992)).

For the purpose of analysis, the material principal axes are arbitrarily chosen to correspond to the global Cartesian axes (i.e. $\theta = 0^\circ$ in Fig. 5). It should be recognised, however, that by virtue of the geometry, the calculations would indeed be as those for the case of general anisotropy when the inclined angle α of the crack is not zero. This inclined angle of the crack is varied from zero to 45° in this study, and for each of angle of inclination, stress intensity factor solutions for relative crack lengths, a/W , ranging from 0.1 to 0.5 are obtained for Examples (a) and (b). The range of a/W considered for Example (c) was 0.15 to 0.30. Since the solutions for these problems

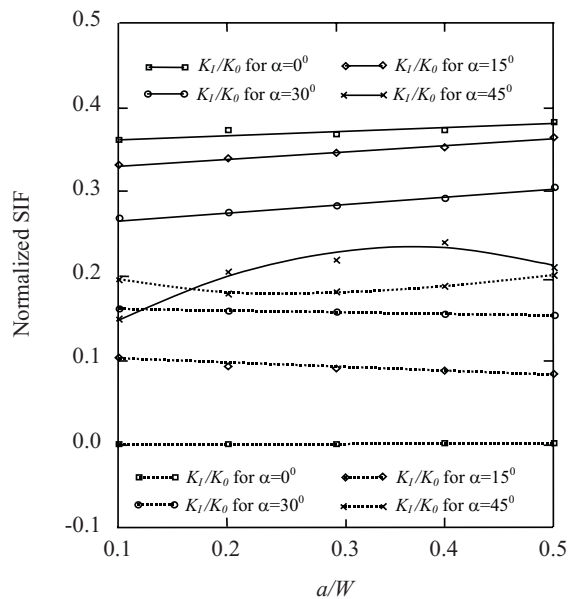


Figure 8 : Variations of the normalised SIF's with relative crack length a/W for the crack tip P-Example (a)

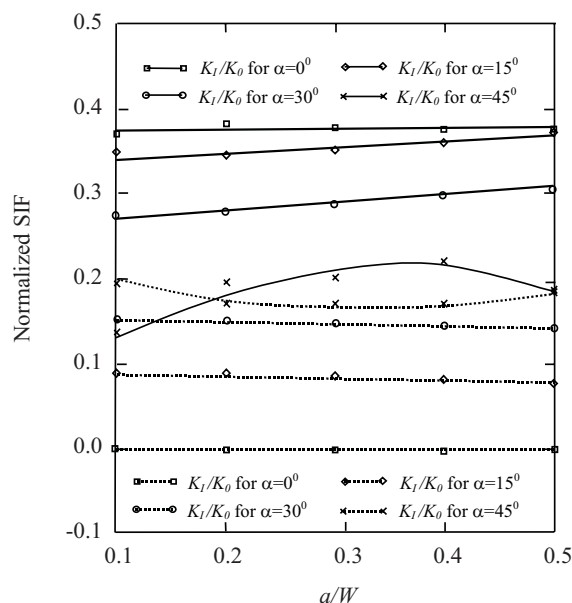


Figure 9 : Variations of the normalised SIF's with relative crack length a/W for the crack tip Q- Example (a)

are not readily available in the literature for comparison, they are also obtained by an alternative means here, namely, the method of superposition.

Figure 6 illustrates the use of the principle of superposition to determine stress intensity factors in linear thermoelastic fracture mechanics. The stress intensity factors for the problem of a cracked plate subjected to thermal loads (problem (A)) can be obtained by treating it as a superposition of two sub-problems: sub-problem (B) and sub-problem (C). Sub-problem (B) corresponds to the same plate with exactly the same displacement and temperature boundary conditions as in problem (A), but it is crack-free. The stress intensity factors are thus zero for this case. Sub-problem (C) is identical to sub-problem (A) in every respect except that it is not subjected to the thermal loads. Instead the crack faces are subjected to the equal and opposite stresses that exist at the prospective crack surfaces in sub-problem (B). The stress intensity factors for the original problem are thus the same as those for sub-problem (C) which is a fracture problem under mechanical loads and for which the BEM is already well established to handle. The determination of the thermal stresses in a two-dimensional crack-free anisotropic solid using BEM has also been previously established, see Shiah and Tan (1999a). Thus the solutions obtained in this study for the three example problems can be checked using this method of superposition. They will now be presented and discussed below, their values are all being normalised with respect to the quantity K_0 , where $K_0 = E_{22}^* \alpha_{22}^* \Theta_0 \sqrt{\pi a}$

4.1 Example (a)

Figure 7 shows a typical BEM mesh discretisation used to solve the temperature field problem as well as the thermoelastic problem shown in Fig. 5(a). The numerical results of the normalised stress intensity factors (SIF's) at crack-tip P (see Fig. 5(a)) as obtained by the direct ETM method in BEM are shown in Table 2. Also shown are the corresponding results obtained by the method of superposition described above. As can be seen, the two sets of solutions are in excellent agreement with one another, with deviations of K_I/K_0 being generally less than one percent. The discrepancies for the values of K_{II}/K_0 are somewhat larger, although they are still generally less than 4 percent, noting that the mode II stress intensity factors are lower in magnitudes. The numerical values of the normalised stress intensity factors for the crack-tip Q are listed in Table 3. Note that for the case when $\alpha = 0^\circ$, the values for both the crack tips will be the same for a given crack size, hence they are not presented here. Again, the agreement between the solutions obtained directly using the ETM and those obtained using the method of superposition, is excellent indeed.

The variations of the normalised SIF's with relative crack size for tip P and tip Q are shown in Fig. 8 and Fig. 9, respectively, for the various angles of inclination of the crack considered. It is worth noting that they change only very gradually and in a linear manner with relative crack size for the range of crack sizes treated, except for the case when $\alpha = 45^\circ$.

Table 2 : Normalized SIF's for the crack tip P — Example (a)

a	$\frac{a}{W}$	K_I/K_0			K_{II}/K_0		
		Direct ETM	Super-pos'n	%Diff	Direct ETM	Super-pos'n	%Diff
0°	0.1	0.361	0.357	1.0	0.000	0.000	—
	0.2	0.371	0.371	0.0	0.000	0.000	—
	0.3	0.367	0.362	1.2	0.001	0.001	—
	0.4	0.372	0.369	0.6	0.002	0.001	—
	0.5	0.381	0.379	0.6	0.002	0.002	—
15°	0.1	0.331	0.332	0.4	0.104	0.108	3.8
	0.2	0.339	0.337	0.7	0.093	0.089	3.7
	0.3	0.345	0.343	0.6	0.089	0.086	3.4
	0.4	0.351	0.350	0.4	0.088	0.086	2.7
	0.5	0.363	0.361	0.4	0.084	0.082	2.7
30°	0.1	0.268	0.269	0.1	0.161	0.155	3.7
	0.2	0.275	0.275	0.0	0.159	0.153	3.5
	0.3	0.282	0.282	0.0	0.158	0.153	3.1
	0.4	0.292	0.292	0.0	0.155	0.151	2.5
	0.5	0.305	0.305	0.0	0.154	0.150	2.3
45°	0.1	0.148	0.150	1.4	0.195	0.188	3.7
	0.2	0.204	0.205	0.8	0.178	0.172	3.0
	0.3	0.219	0.220	0.7	0.181	0.176	2.9
	0.4	0.239	0.240	0.5	0.187	0.182	2.3
	0.5	0.208	0.209	0.5	0.200	0.197	1.7

Table 3 : Normalized SIF's for the crack tip Q — Example (a)

a	$\frac{a}{W}$	K_I/K_0			K_{II}/K_0		
		Direct ETM	Super-pos'n	%Diff	Direct ETM	Super-pos'n	%Diff
0°	0.1	0.361	0.357	1.0	0.000	0.000	—
	0.2	0.371	0.371	0.0	0.000	0.000	—
	0.3	0.367	0.362	1.2	0.001	0.001	—
	0.4	0.372	0.369	0.6	0.002	0.001	—
	0.5	0.381	0.379	0.6	0.002	0.002	—
15°	0.1	0.334	0.336	0.4	0.090	0.094	4.4
	0.2	0.339	0.337	0.7	0.090	0.087	3.6
	0.3	0.344	0.342	0.6	0.087	0.084	3.2
	0.4	0.351	0.349	0.5	0.083	0.081	2.7
	0.5	0.362	0.360	0.4	0.080	0.078	2.6
30°	0.1	0.269	0.270	0.2	0.159	0.152	4.1
	0.2	0.274	0.274	0.0	0.157	0.152	3.5
	0.3	0.281	0.281	0.0	0.155	0.150	3.1
	0.4	0.290	0.291	0.0	0.152	0.148	2.6
	0.5	0.303	0.303	0.0	0.149	0.145	2.4
45°	0.1	0.147	0.149	1.4	0.195	0.188	3.7
	0.2	0.196	0.199	0.8	0.174	0.168	3.1
	0.3	0.208	0.210	0.7	0.174	0.168	3.2
	0.4	0.224	0.226	0.5	0.174	0.169	2.6
	0.5	0.188	0.190	0.5	0.186	0.183	1.9

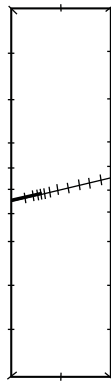


Figure 10 : Typical BEM mesh for Example (b)

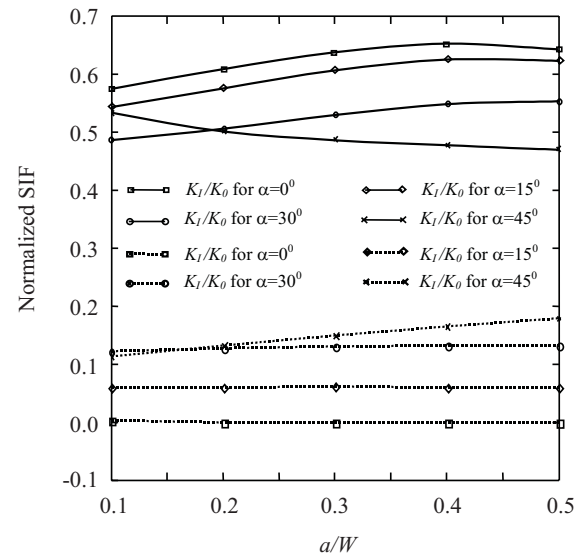


Figure 11 : Variations of the normalised SIF's with relative crack length a/W - Example (b)

4.2 Example (b)

For Example (b), a typical BEM mesh discretisation used in the BEM analysis, is shown in Fig. 10. A comparison of the normalised SIF's at the tip of the inclined edge crack obtained using the direct ETM technique and those obtained using the superposition method is shown in Table 4. The discrepancies between the two sets of results for K_I/K_0 are, again, all within one percent. The relatively greater percentage discrepancies for K_{II}/K_0 can be attributed to their small magnitudes. The variations of the SIF's with relative crack size, a/W , are shown

in Fig. 11. Of interest to note is that, other than for the case of crack inclination angle $\alpha = 45^\circ$, the normalised value of the mode II SIF, K_{II}/K_0 , remains, for all practical purposes, constant with changes in the relative crack length. As to be expected the mode I stress intensity factor is greater than that in Example (a) of the central inclined crack for the same crack size.

Table 4 : Normalized SIF's — Example (b)

a	$\frac{a}{W}$	K_I/K_0			K_{II}/K_0		
		Direct ETM	Super-pos'n	%Diff	Direct ETM	Super-pos'n	%Diff
0°	0.1	0.574	0.571	0.6	0.003	0.003	—
	0.2	0.608	0.605	0.5	0.000	0.000	—
	0.3	0.638	0.635	0.5	0.000	0.000	—
	0.4	0.653	0.650	0.5	0.000	0.000	—
	0.5	0.643	0.640	0.5	0.000	0.001	—
15°	0.1	0.541	0.538	0.4	0.060	0.058	6.3
	0.2	0.577	0.574	0.4	0.061	0.059	5.3
	0.3	0.607	0.605	0.4	0.061	0.059	4.5
	0.4	0.626	0.623	0.4	0.061	0.059	3.9
	0.5	0.622	0.620	0.4	0.060	0.058	3.4
30°	0.1	0.490	0.491	0.0	0.123	0.116	5.5
	0.2	0.506	0.506	0.0	0.128	0.122	4.5
	0.3	0.532	0.532	0.0	0.130	0.125	4.0
	0.4	0.550	0.549	0.0	0.132	0.127	3.6
	0.5	0.554	0.553	0.2	0.133	0.129	3.3
45°	0.1	0.533	0.537	0.8	0.113	0.106	6.8
	0.2	0.502	0.506	0.7	0.133	0.126	5.0
	0.3	0.488	0.491	0.7	0.150	0.144	4.1
	0.4	0.478	0.481	0.6	0.165	0.159	3.6
	0.5	0.470	0.472	0.4	0.179	0.173	3.3

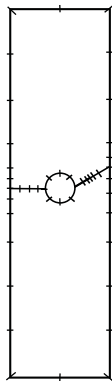


Figure 12 : Typical BEM mesh for Example (c)

4.3 Example (c)

Figure 12 shows a typical mesh used in the BEM analysis for solving the problem in Fig. 5(c). The computed normalised SIF's are listed in Table 5, where it can be seen again that the results obtained by the ETM technique are in excellent agreement with those computed using the method of superposition. The relatively larger percentage discrepancies between these solutions for the mode II SIF's can again be attributed largely to their smaller values. The variations of the normalised SIF's with relative crack length, a/W , are shown in Fig. 13. It is evident that the change in the SIF's becomes generally more pronounced with a change in the relative crack size in this

Table 5 : Normalized SIF's — Example (c)

a	$\frac{a}{W}$	K_I/K_0			K_{II}/K_0		
		Direct ETM	Super-pos'n	%Diff	Direct ETM	Super-pos'n	%Diff
0°	0.15	0.524	0.526	0.2	0.001	0.001	—
	0.20	0.496	0.493	0.6	0.000	0.000	—
	0.25	0.477	0.475	0.4	0.000	0.000	—
	0.30	0.473	0.470	0.5	0.000	0.000	—
15°	0.15	0.516	0.518	0.5	0.063	0.061	4.3
	0.20	0.476	0.476	0.0	0.083	0.080	4.1
	0.25	0.451	0.450	0.2	0.102	0.099	3.2
	0.30	0.442	0.440	0.4	0.118	0.115	2.6
30°	0.15	0.471	0.473	0.4	0.108	0.102	5.6
	0.20	0.463	0.463	0.0	0.052	0.048	5.8
	0.25	0.425	0.427	0.4	0.093	0.088	5.5
	0.30	0.406	0.406	0.0	0.115	0.110	4.5
45°	0.15	0.500	0.507	1.4	0.097	0.094	3.8
	0.20	0.419	0.424	1.3	0.143	0.138	3.5
	0.25	0.229	0.232	1.3	0.241	0.234	2.9
	0.30	0.212	0.215	1.4	0.264	0.259	1.9

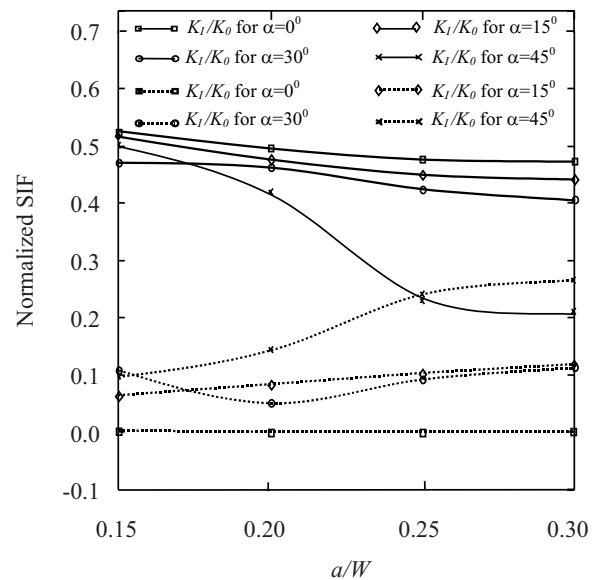


Figure 13 : Variations of the normalised SIF's with relative relative crack length, a/W - Example (c)

problem, particularly when the inclined angle of the crack is greater than 30°.

5 Conclusions

As in BEM for isotropic elasticity, the volume integral term associated with thermal loading in coupled anisotropic thermoelasticity can be analytically transformed into surface ones in the boundary integral equation. This would restore the BEM

for such problems in anisotropic elasticity as a truly boundary solution technique. The main steps in this exact transformation method (ETM) have been presented in this paper. The method can be applied to solving fracture problems without any further modifications or approximations to the BEM algorithm. This has been demonstrated by three example problems and the stress intensity factors for them have been presented. Due to the scarcity of solutions for these problems in the literature, the numerical results obtained from the ETM technique have been compared with those computed using the method of superposition and excellent agreement between them were established.

References

- Camp, C. V.; Gipson, G. S.** (1992): *Boundary Element Analysis of Nonhomogeneous Biharmonic Phenomena*. Springer-Verlag, Berlin.
- Danson, D.** (1983): Linear isotropic elasticity with body forces. In Brebbia, C. A.(Ed): *Progress in boundary element methods*. Pentech Press, London.
- Deb, A.; Banerjee, P. K.** (1990): BEM for general anisotropic 2d elasticity using particular integrals. *Commun. Appl. Num. Mech.*, vol. 6, pp. 111–119.
- Deb, A.; Henry Jr., D. P.; Wilson, E. B.** (1991): Alternative BEM formulation for 2d and 3d thermoelasticity. *Int. J. Solids Struct.*, pp. 1721–1738.
- Gipson, G. S.; Camp, C. V.** (1985): Effective use of Monte Carlo quadrature for body force integrals occurring in integral form of elastostatics. In *Proc. 7th Int. Conf. On Boundary Elements*, pp. 17–26.
- Kamel, M.; Liaw, B. M.** (1981): Boundary element analysis of cracks at a fastener hole in an anisotropic sheet. *Int. J. Fracture*, vol. 50, pp. 263–280.
- Lachat, J. C.** (1975): *Further development of the boundary integral technique for elastostatics*. Ph.D. Thesis, Southampton University.
- Lekhnitskii, S. G.** (1981): *Theory of Elasticity of an Anisotropic Body*. Mir Publishers, Moscow.
- Pan, E.; Amadei, B.** (1996): Fracture mechanics analysis of cracked 2d anisotropic media with a new formulation of the boundary element method. *Int. J. Fracture*, vol. 77, pp. 161–174.
- Rizzo, F. L.; Shippy, D. J.** (1977): An advanced boundary integral equation method for three-dimensional thermoelasticity. *Int. J. Numerical Methods Engng.*, vol. 11, pp. 1753–1768.
- Shiah, Y. C.; Tan, C. L.** (1998): BEM treatment of two-dimensional anisotropic field problems by direct domain mapping. *Engng. Analysis with Boundary Elements*, vol. 20, pp. 347–351.
- Shiah, Y. C.; Tan, C. L.** (1998): Calculation of interior point stresses in 2-d boundary element analysis of anisotropic bodies with body forces. *J. Strain Analysis for Engng. Design*, vol. 34, pp. 117–128.
- Shiah, Y. C.; Tan, C. L.** (1999): Determination of interior point stresses in two-dimensional BEM thermoelastic analysis of anisotropic bodies. *Int. J. Solids Struct.*, vol. 37, pp. 809–829.
- Shiah, Y. C.; Tan, C. L.** (1999): Exact boundary integral transformation of the thermoelastic domain integral in BEM for general 2d anisotropic elasticity. *Comput. Mech.*, vol. 23, pp. 87–96.
- Snyder, M. D.; Cruse, T. A.** (1975): Boundary integral equation analysis of cracked anisotropic plates. *Int. J. Fracture*, vol. 11, pp. 315–328.
- Sollero, P.; Aliabadi, M. H.** (1993): Fracture mechanics analysis of anisotropic composite laminates by the boundary element method. *Int. J. Fracture*, vol. 64, pp. 269–284.
- Tan, C. L.** (1983): Boundary integral equation stress analysis of a rotating disc with corner crack. *J. Strain Analysis*, vol. 18, pp. 231–237.
- Tan, C. L.; Gao, Y. L.** (1992): Boundary element analysis of plane anisotropic bodies with stress concentration and cracks. *Composite struct.*, vol. 20, pp. 17–28.
- Tan, C. L.; Gao, Y. L.; Afagh, F. F.** (1992): Anisotropic stress analysis of inclusion problems using the boundary integral equation method. *J. Strain Analysis*, vol. 27, no. 2, pp. 67–76.
- Tan, C. L.; Shiah, Y. C.** (1999): Two-dimensional BEM thermoelastic analysis of cracked anisotropic bodies. In Aliabadi, M.(Ed): *Proc. Int. Conf. BEM Techniques*, pp. 41–50.
- Zhang, J. J.; Tan, C. L.; Afagh, F. F.** (1996): An argument redefinition procedure in the BEM for 2d anisotropic elastostatics with body forces. In Meguid, S. A.(Ed): *Proc. Symp. Mechanics in Design*, volume 1, pp. 349–358.
- Zhang, J. J.; Tan, C. L.; Afagh, F. F.** (1996): A general exact transformation of body-force volume integral in BEM for 2d anisotropic elasticity. *Comput. Mech.*, vol. 19, pp. 1–10.
- Zhang, J. J.; Tan, C. L.; Afagh, F. F.** (1997): Treatment of body-force volume integrals in BEM by exact transformation for 2d anisotropic elasticity. *Int. J. Numerical Methods Engng.*, vol. 40, pp. 89–109.

